water

MDPI

Article

Advanced Method to Capture the Time-Lag Effects between Annual NDVI and Precipitation Variation Using RNN in the Arid and Semi-Arid Grasslands

Taosuo Wu [1,2,3], Feng Feng [4,*], Qian Lin [5] and Hongmei Bai [1]

1 School of Microelectronics, Tianjin University, Tianjin 300072, China
2 School of Physics and Electronic Information, Hulunbuir College, Hulunbuir 021008, China
3 Tianjin Key Laboratory of Imaging and Sensing Microelectronic Technology, Tianjin University, Tianjin 300072, China
4 Department of Electronics, Carleton University, Ottawa, ON K1S5B6, Canada
5 College of Physics and Electronic Information Engineer, Qinghai Nationalities University, Xining 810000, China
* Correspondence: fengfeng@doe.carleton.ca; Tel.: +1-613-890-9207

Received: 22 July 2019; Accepted: 24 August 2019; Published: 28 August 2019

Abstract: The latest research indicates that there are time-lag effects between the normalized difference vegetation index (NDVI) and the precipitation variation. It is well known that the time-lags are different from region to region, and there are time-lags for the NDVI itself correlated to the precipitation. In the arid and semi-arid grasslands, the annual NDVI has proved not only to be highly dependent on the precipitation of the concurrent year and previous years, but also the NDVI of previous years. This paper proposes a method using recurrent neural network (RNN) to capture both time-lags of the NDVI with respect to the NDVI itself, and of the NDVI with respect to precipitation. To quantitatively capture these time-lags, 16 years of the NDVI and precipitation data are used to construct the prediction model of the NDVI with respect to precipitation. This study focuses on the arid and semi-arid Hulunbuir grasslands dominated by perennials in northeast China. Using RNN, the time-lag effects are captured at a 1 year time-lag of precipitation and a 2 year time-lag of the NDVI. The successful capture of the time-lag effects provides significant value for the accurate prediction of vegetation variation for arid and semi-arid grasslands.

Keywords: time-lag effects; recurrent neural network; NDVI; precipitation

1. Introduction

The interannual variability of vegetation can be well-described by the remotely sensed normalized difference vegetation index (NDVI), which is derived from satellite optical-infrared remote sensing [1–6]. In arid and semi-arid regions, the annual NDVI is highly sensitive to the interannual variability of precipitation [7–10]. Recently, the annual NDVI has proved to be highly dependent on the precipitation of the concurrent year and the previous year [7,8,11]. The dependence of vegetation variation on precipitation is referred to as "time-lag effects" [8,12]. These effects have been observed in different arid and semi-arid regions [12].

In order to understand time-lag effects, the time-lags have to be investigated both qualitatively and quantitatively. It is a common understanding that the vegetation variation is correlated not only to the precipitation of the concurrent year and previous years, but also to the vegetation itself in previous years. It is desirable to have quantitatively investigated time-lags for the further understanding of time-lag effects.

Reviews on the time-lag effects of global vegetation variation responses to climate change have been reported qualitatively [12]. The time-lags between the NDVI and precipitation in arid to semi-arid regions have been reported quantitatively in the literature [7,8]. Obviously, the time-lags vary in different regions [12]. It is also well known that there are time-lags for the NDVI itself correlated to the precipitation. Consequently, how to accurately capture time-lags of vegetation response with respect to both the vegetation itself and precipitation remains an open topic.

In the existing literature, researchers have investigated the relationship between the NDVI and precipitation using the multiple linear regression (MLR) technique [8,13], back propagation neural network (BPNN) and support vector machine (SVM) [14,15]. These methods can effectively model linear and nonlinear data characteristics of the NDVI–precipitation relationship. However, influenced by time-lag effects, there are time-lags for the NDVI response to precipitation [12]. The NDVI–precipitation relationship is the result of dynamical interactions exerted over a wide range of the temporal scale [16,17]. The methods used in the literature are considered as static and memoryless networks, and lack the ability to examine the temporal dimension of data and to capture the time-lag effects between the NDVI and precipitation [18]. Therefore, to accurately capture the time-lag effects, it is necessary to consider a dynamic method (i.e., dynamic neural network) that can be used to determine the temporal relationship between the NDVI and precipitation.

Recurrent neural network (RNN) is one of the effective dynamic neural networks characterized by internal self-connections. Both hidden and output layers of RNN have internal time-delay feedback loops which are fully connected. RNN provides a very elegant way of dealing with (time) sequential data that embody correlations between data points that are close in the sequence [19,20]. RNN can accurately learn and represent the dynamic input–output relationship for time series prediction, and has been widely used in data classification, computational neuroscience and machine learning applications [19–21]. Recently, RNN has been used to capture temporal dependencies in multivariate time series to perform predictions [22].

In this paper, RNN is introduced to capture the time-lag effects between the NDVI and precipitation. The RNN can accurately predict output behaviors by not only the current and past inputs but also the output behaviors in past periods [20,21]. This study focuses on the arid and semi-arid Hulunbuir grasslands of northeast China (46°55′–50°50′ N; 115°00′–120°29′ E). The NDVI and the precipitation data from 2000 to 2015 are used to construct the prediction model of the NDVI with respect to precipitation, for the further understanding of time-lag effects. The proposed technique can successfully capture the time-lag effects between the NDVI and precipitation in the arid and semi-arid Hulunbuir grasslands of northeast China. The successful capture of the time-lag effects provides significant value for the accurate prediction of vegetation variation.

2. Materials and Methods

2.1. Study Region and Data

2.1.1. Study Region and Vegetation Structure

The study region (Hulunbuir grasslands, 46°55′–50°50′ N and 115°00′–120°29′ E) (Figure 1), which includes the meadow steppe, typical steppe, and desert steppe from east to west, is characterized by arid and semi-arid conditions (Figure 1). Located in the eastern section of the Inner Mongolia Autonomous Region of China, the area of the study region is about 8×10^4 km^2 with a mean elevation of 650–750 m and is covered mostly by natural vegetation. It has the typical temperate continental monsoon climate with an average annual temperature of −0.7 °C. The annual precipitation is 292.1 mm and the main part of the precipitation occurs from June to August [23]. The vegetation variation in the arid and semi-arid grasslands is more sensitive to precipitation than temperature in the grass-growing season [24]. The spatial vegetation variation has proved to be correlated to the amount of precipitation [25]. The mean annual precipitation (mm yr^{-1}) increases from less than 235 mm yr^{-1} in the western parts to more than 330 mm yr^{-1} in the eastern parts of the study area.

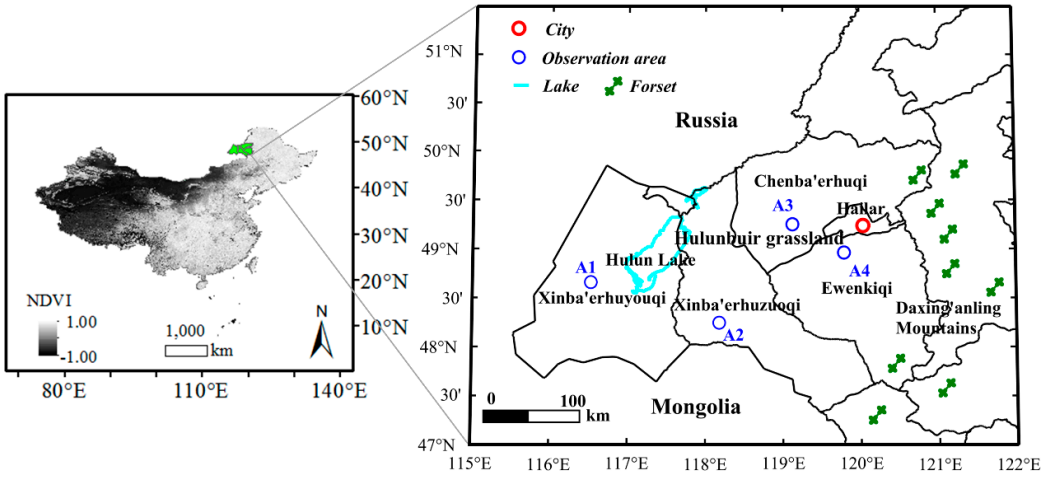

Figure 1. Location of study region.

As shown in Figure 2, the land cover data of the study area were extracted from the GlobCover 2009 provided by the European Space Agency (ESA) and Université Catholique de Louvain (http://due.esrin.esa.int/page_globcover.php). The study region is divided into four sub-regions, i.e., Xinba'erhuyouqi (A1), Xinba'erhuzuoqi (A2), Chen ba'erhuqi (A3) and Ewenkiqi (A4). A1 to A4 are covered by multiple land cover types, including grassland, forest, water bodies, bare areas and other types (Table 1).

Table 1. Land cover data of study region.

Sub-Region	Grassland (%)	Forest (%)	Water Bodies (%)	Other Types (%)
A1	67.36 *	-	8.53	24.11 ***
A2	89.34	3.94	0.51	6.21
A3	88.69 **	3.10	2.58	5.63
A4	60.60	24.36	8.88	6.16

* The proportion of sparse (<15%) vegetation is 42.23%, ** the proportion of sparse (<15%) vegetation is 38.67%, *** the proportion of bare areas is 23.48%.

As the typical steppe, located in the western part of the study region, A1 is dominated by *Stipa krylovii* Roshev, *Leymus chinensis* (Trin.) Tzvel, *Allium polyrhizum* Turcz. ex Regel and *Cleistogenes squarrosa* (Trin.) Keng. Located at the central part of the study region, A2 is the desert steppe and is dominated by *Stipa grandis* P. Smirn, *Leymus chinensis* (Trin.) Tzvel, *Artemisia frigida* Willd and *Cleistogenes squarrosa* (Trin.) Keng. The meadow steppe (A3 and A4), located in the eastern part of the study region, is dominated by *Leymus chinensis* (Trin.) Tzvel, *Stipa Baicalensis* Roshev and *Stipa grandis* P. Smirn [26].

2.1.2. The NDVI and Precipitation Data Set

The monthly composite MODIS NDVI data set (MODIS/Terra, MOD09GA, Version 5) during the period of February 2000–December 2015 were obtained from the International Scientific and Technical Data Mirror Site, Computer Network Information Center, Chinese Academy of Sciences (http://www.gscloud.cn). These NDVI data were processed by the maximum value composite (MVC) to eliminate the effects of cloud cover, dust and aerosols from atmospheric conditions on the NDVI images. In this study region, the main part of the annual precipitation occurs in the growing season (from June to August). The annual NDVI has proved to be highly dependent on precipitation. Therefore, the annual NDVI in this study region can be represented by the mean monthly value of the NDVI in the growing season [23]. In addition, the monthly precipitation data of the four sub-regions were provided by the local meteorological service in A1–A4. Since the percentage of the annual precipitation (about

76.50%) is concentrated in the growing season from June to August, the mean monthly precipitation in the growing season can be represented by the mean values from June to August [23].

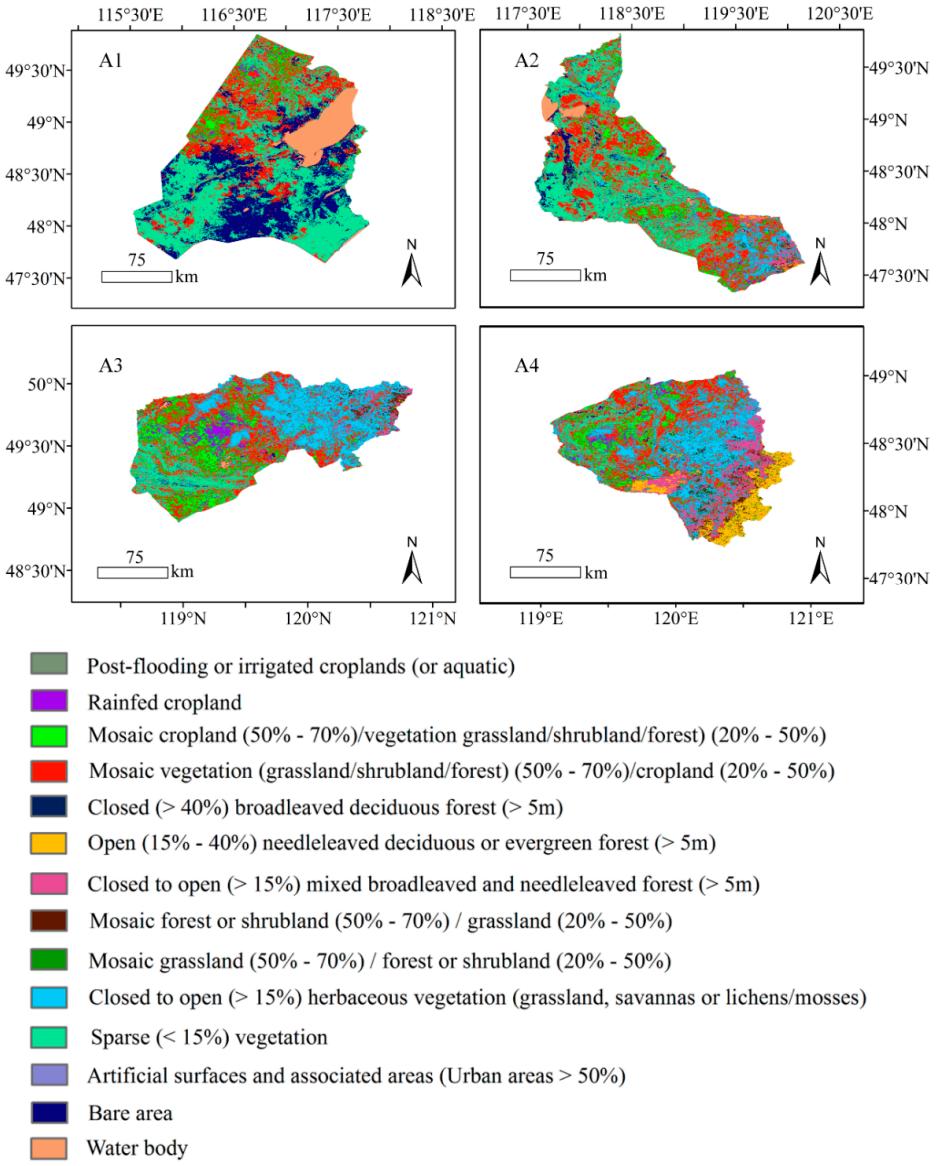

Figure 2. Land cover types of study region.

2.2. Methods

Artificial neural networks (ANNs) are robust computing systems for modeling complex relationships between sets of inputs and outputs [27]. Generally, the structure of ANNs consists of an input layer, one or more hidden layers and an output layer of the interconnected "neurons", which communicate with each other by exchanging messages. BPNN is one of the most popular ANNs, which is a typical feedforward neural network. Time-delay neural network (TDNN) is developed from the general feedforward neural network (i.e., BPNN) by adding a set of input time-delay units, which can be used to find the potentially temporal relationship among inputs [28]. RNN is further developed based on TDNN, which consists of not only the inputs with a set of time-delay units but also feedback from outputs with another set of time-delay units. In this paper, the RNN is used to model the time domain behaviors of the NDVI versus precipitation in order to predict the NDVI with given values of precipitation. In addition, to intuitively know the ability of RNN to represent the NDVI–precipitation relationship, we compare RNN with BPNN, TDNN and simple statistical techniques (i.e., MLR) [8,13].

2.2.1. BPNN

As one of the most popular ANNs, BPNN belongs to a typical feedforward neural network (Figure 2a) [29,30]. The data flow of BPNN is in one direction and the model output is obtained solely based on the current set of inputs [31,32]. The training procedure of BPNN uses backward error propagation, which is an iterative gradient descent algorithm designed to minimize the mean squared error between network predicted outputs and training set values [33]. In this study, the training algorithm of BPNN is Levenberg–Marquardt, which is used to train BPNN based on the observed data (the observed NDVI) and the model output (the predicted NDVI). The activation functions in the hidden and output layers used in this study are sigmoid and linear types, respectively.

As shown in Figure 3a, $P(t)$ and $I_N(t)$ represent the time series of precipitation and the NDVI. The observed precipitation and NDVI data from 2000 to 2015 in the four sub-regions are used to train the BPNN model. The data are divided into two sets, which are the training set (80%) and the testing set (20%). For sub-regions A1 and A2, a three-layer neural network of one hidden layer with three hidden neurons was found to be the optimal structure with the best accuracy for the NDVI prediction with respect to precipitation, and a three-layer neural network of one hidden layer with four hidden neurons was found to be the optimal structure for A3 and A4.

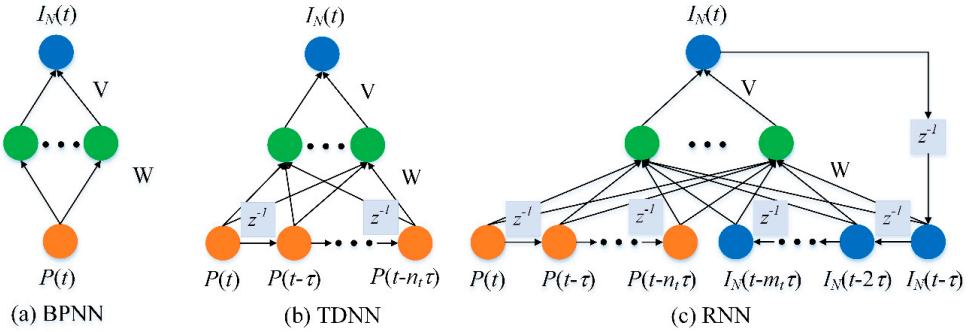

Figure 3. Architectures of (**a**) the back propagation neural network (BPNN), (**b**) the time-delay neural network (TDNN) and (**c**) the recurrent neural network (RNN) (z^{-1} represents the time-delay unit, V and W are weight connections for linking neurons).

2.2.2. TDNN

As a dynamical ANN, TDNN is developed from a general feedforward neural network, such as BPNN, and commonly used for input–output modeling of nonlinear dynamical systems [28]. TDNN has an input time-delay unit, which can be used to store the events of inputs across time [31]. Figure 3b shows the detailed structure of the TDNN model for predicting the NDVI with respect to precipitation. The TDNN model for predicting the NDVI with respect to precipitation is defined as:

$$I_N(t) = f_{\mathrm{TDNN}}[P(t), P(t-\tau) \ldots P(t-n_t\tau)] \quad (1)$$

where $P(t)$ represents the time series of the precipitation as the input of TDNN. $I_N(t)$ represents the time series of the NDVI as the output of TDNN. τ represents the value of time-delay; n_t represents the total number of time-delays used in TDNN; f_{TDNN} (•) represents the nonlinear mapping function for TDNN. The precipitation data and NDVI data from 2000 to 2015 in A1–A4 are divided into training data (80%) and testing data (20%) for training the four TDNN models, respectively. The optimal number of time-delays and the optimal number of neurons in the one hidden layer were determined to be one and six, respectively, for all of the TDNN models.

2.2.3. RNN

RNN has been demonstrated it has good memory ability using time-delay units. RNN can be easily and efficiently applied to time series prediction [34]. The architecture of the RNN model used

in this study is shown in Figure 3c. RNN consists of input, hidden and output layers, and produces recurrent connections from the output which may delay several unit times to form new inputs using a time-delay unit (z^{-1}) [20,21,35]. As shown in Figure 3c, RNN has a good memory capability using time-delay units to predict the output behaviors by not only the input in the current and the past periods, but also the output in the past periods. Therefore, the RNN for predicting NDVI with respect to precipitation is formulated as:

$$I_N(t) = f_{\mathrm{RNN}}[P(t), P(t-\tau)\ldots P(t-n_t\tau); I_N(t-\tau), I_N(t-2\tau)\ldots, I_N(t-m_t\tau)] \quad (2)$$

where $P(t)$ and $I_N(t)$ represent the time series of precipitation and the NDVI as the input and output of the RNN model at discrete time step t, respectively; τ represents the value of the time-delay; n_t and m_t represent the total number of time-delays used in the input layer and output layer of the RNN model, respectively; $f_{\mathrm{RNN}}(\bullet)$ is the nonlinear mapping function for RNN.

In this study, the NDVI prediction model is constructed by RNN. As shown in Figure 3c, $P(t)$ and $I_N(t)$ are the input and output, respectively. The observed precipitation and NDVI data from 2000 to 2015 in the sub-regions are used to train the RNN. The data are randomly divided into two sets by time. The two sets are the training set (80%) and the testing set (20%), respectively. The three-layer neural network structure is used as the RNN structure. The number of hidden neurons of the RNN model is continuously increased until the minimum training and testing errors are obtained. After the suitable number of hidden neurons is determined, different combinations of different numbers of the input and output time-delays are tried to find the best combination. After training, a three-layer neural network structure with one hidden layer (seven hidden neurons), one input time-delay ($P(t-1)$ is considered an input) and two output time-delays ($I_N(t-1)$, $I_N(t-2)$ are considered as outputs) was found to be the optimal structure for the NDVI prediction with respect to precipitation in the four sub-regions.

To quantify the applicability, reliability and accuracy of the MLR, BPNN and RNN models, the mean absolute error (*MAE*), root mean square error (*RMSE*) and mean absolute percentage error (*MAPE*) are often used to measure the predictive performance of a model [14]. The *MAE*, *RMSE* and *MAPE* are defined as:

$$MAE = \frac{1}{n}\sum_{i=1}^{n}\left|y_i - d_i\right| \quad (3)$$

$$RMSE = \sqrt{\frac{1}{n}\sum_{i=1}^{n}\left|y_i - d_i\right|^2} \quad (4)$$

$$MAPE(\%) = \frac{1}{n}\sum_{i=1}^{n}\left|\frac{y_i - d_i}{d_i}\right| \quad (5)$$

where n denotes the number of data sets; y_i and d_i represent the observed and predicted NDVI in the growing season of the ith year.

3. Results and Discussion

Trained with the same data, the RNN used in this study is compared with MLR, BPNN and TDNN. Figure 4 shows the prediction results of the NDVI with given values of precipitation for the four comparative models (MLR, BPNN, TDNN and RNN) obtained for the four sub-regions (A1–A4). In Figure 4, R^2 means the determination coefficient of assessing a possible linear association between the predicted NDVI and the observed NDVI. The R^2 values of the RNN were from 0.897 to 0.960, which is obviously higher than those of MLR, BPNN and TDNN, indicating that RNN has better fitness than the other three modeling methods. In addition, the error parameters of MLR, BPNN, TDNN and RNN for predicting the NDVI are shown in Figure 5. It was found that RNN has the best performance among the four comparative models in predicting the NDVI with respect to precipitation in terms of *MAE*, *RMSE* and *MAPE* in the four sub-regions. The results indicate that the RNN model has better

predicting accuracy (*MAE*) and stronger robustness (*RMSE* and *MAPE*) in the NDVI predictions than MLR, BPNN and TDNN.

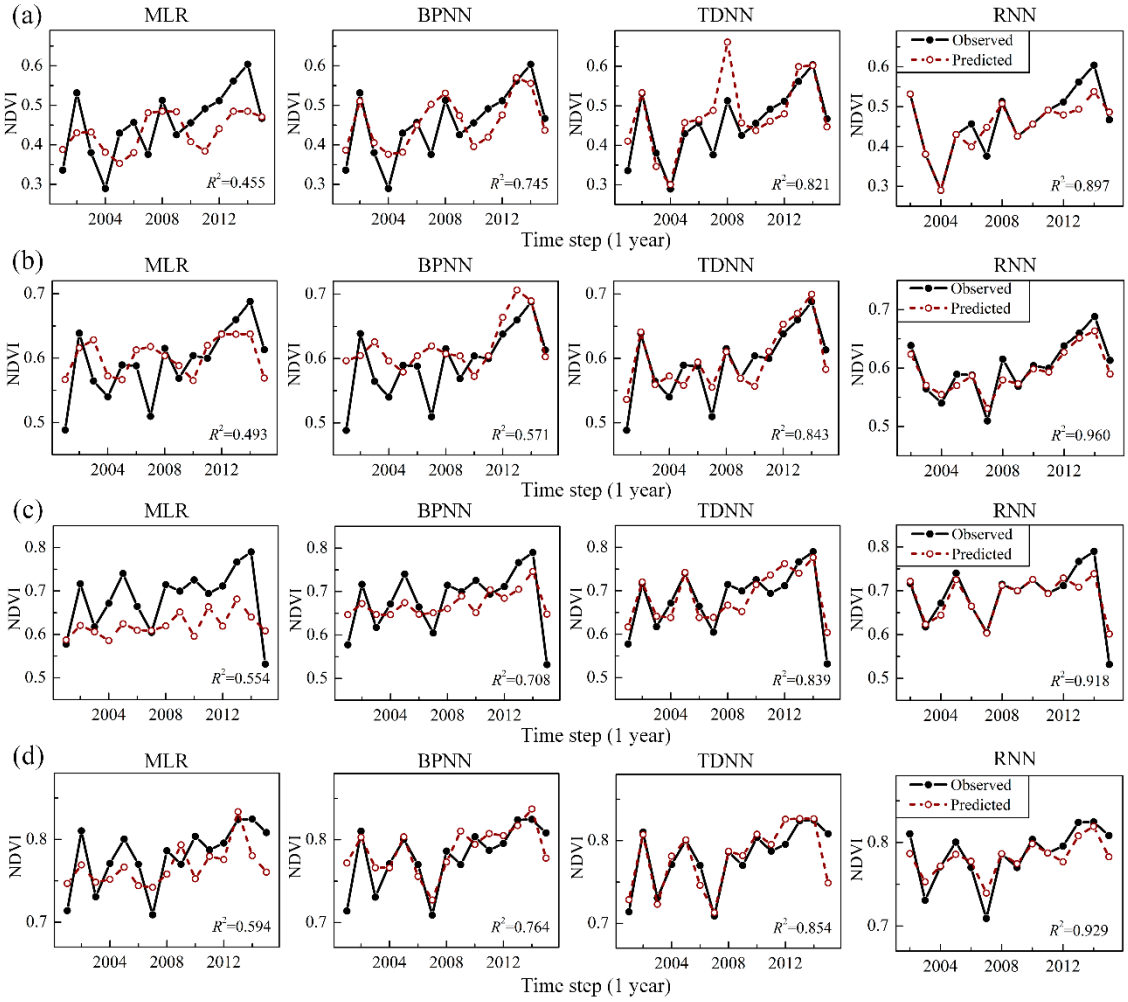

Figure 4. The comparisons of the observed normalized difference vegetation index (NDVI) data and predicted NDVI data for (**a**) A1, (**b**) A2, (**c**) A3 and (**d**) A4 from the multiple linear regression (MLR), BPNN, TDNN and RNN models, respectively. $I_N(t-1)$, $I_N(t-2)$ are considered as inputs in the RNN model.

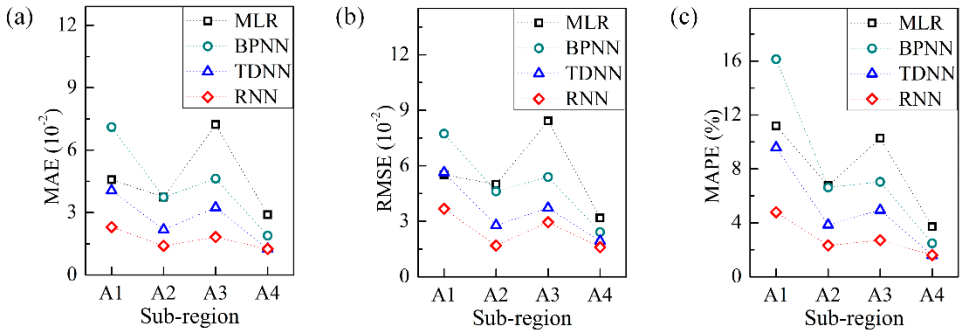

Figure 5. Error parameters (**a**) mean absolute error (*MAE*), (**b**) root mean square error (*RMSE*) and (**c**) mean absolute percentage error (*MAPE*) of the MLR, BPNN, TDNN and RNN models for predicting the NDVI.

From Figures 4 and 5, we noticed that RNN performs better than the other three prediction models. This reveals that the responses of the NDVI to precipitation and the NDVI itself have certain time-lags, which can be successfully and accurately captured by RNN. The results of the NDVI prediction demonstrate that the optimal RNN model with one input time-delay ($P(t-1)$ is considered an input) and two output time-delays ($I_N(t-1)$, $I_N(t-2)$ are considered as outputs) produces the best performance for predicting the NDVI for A1–A4. The time-delay unit in this study is 1 year. Since the input of RNN is precipitation, one input time-delay in RNN means 1 year time-lag of precipitation. Since the output of RNN is the NDVI, two output time-delays in RNN mean 2 year time-lags of the NDVI. Therefore, the 1 year time-lag of precipitation and the 2 year time-lags of the NDVI as the time-lag effects for the NDVI in the current year are successfully captured using RNN over the study region. In other words, the NDVI of the current year is closely related to the precipitation of the current year and 1 previous year, and the NDVI of 2 previous years.

In the study region, the water availability during the early summer (i.e., May and June) of the previous year could control the germination response, which could in turn affect the vegetation growth (i.e., an increase or decrease in seed) a year later [8,36,37]. Therefore, the relation between the germination and production of seeds during the growing season in the previous year and the response of grasslands in the concurrent year can explain the time-lag effect of a 1 year time-lag of precipitation.

In addition, as described in Section 2.1, typical species in the study region include *Leymus chinensis* (Trin.) Tzvel, *Stipa krylovii* Roshev, *Stipa grandis* P. Smirn and *Stipa krylovii* Roshev, which are perennial species. Perennials live for many years. Perennials devote the first year to vegetative growth and building up the reserve of resources, and enter reproductive phase (i.e., seed production) in the second year [38]. Such an explanation would be consistent with the time-lag effect of the 2 year time-lag of the NDVI.

The performances of RNN slightly vary in different land cover types in the study areas (Figures 4 and 5). For instance, we noticed that RNN in sub-region A4 had the best performance among the four sub-regions. RNN in sub-region A2 performed better than A1 and A3. The performance of RNN in sub-region A1 was inferior to those in A2–A4. This indicates that the RNN model cannot successfully capture the time-lag effects between the annual NDVI and precipitation variation in the relatively arid regions of A1 and A3, in which the proportion of sparse (<15%) vegetation and bare areas are relatively high (Table 1). The sparse vegetation and bare soil in these study areas mean low production of seeds, which can affect the accuracy of RNN in capturing the time-lag effects between the annual NDVI and precipitation variation. In contrast, the RNN model worked best in areas with relatively dense vegetation in arid and semi-arid grasslands.

The RNN model used in this study can achieve the best performance for predicting the NDVI among all the modeling techniques tested. Using RNN, the time-lag effects between the NDVI and precipitation can be successfully captured, showing that the NDVI can be well represented by certain time-lags of not only the precipitation but also the NDVI itself in the arid and semi-arid Hulunbuir grasslands of northeast China.

4. Conclusions

This paper has proposed the use of RNN to successfully capture the time-lag effects between the annual NDVI and precipitation. According to the results, RNN can produce much more accurate predictions of the NDVI than TDNN, BPNN and MLR. This reveals that RNN can successfully capture the time-lag effects between the NDVI and precipitation. The 1 year time-lag of precipitation and the 2 year time-lags of the NDVI were captured using RNN over the study region, and these time-lags were consistent with the ecological rules of arid and semi-arid grasslands. The successful capture of the time-lag effects provides significant value for the accurate prediction of vegetation variation in arid and semi-arid grasslands.

Author Contributions: Investigation, T.W. and H.B.; Methodology, F.F.; Writing—original draft, T.W.; Writing—review and editing, F.F. and Q.L.; T.W. and F.F. reviewed this paper.

Funding: This research was funded by National Natural Science Foundation of China (No. 61504092), in part by National 973 Program of China (No. 61331901), in part by Qingdao National Laboratory for Marine Science and Technology of China (No. QNLM2016ORP0411),in part by the National Key R&D Plan (No. 2016YFA0202200), in part by the Tianjin Research Program of Application Foundation and Advanced Technology (No. 15JCQNJC01200)and in part by the AoShan Talents OS (outstanding scientist) Program supported by Qingdao National Laboratory for Marine Science and Technology (No. 2017ASTCP-OS03).

Conflicts of Interest: The authors declare no conflict of interest.

References

1. Zhong, F.; Cheng, Q.; Ge, Y. Relationships between spatial and temporal variations in precipitation, climatic indices, and the normalized differential vegetation index in the upper and middle reaches of the Heihe river basin, Northwest China. *Water* **2019**, *11*, 1394. [CrossRef]
2. Ibrahim, Y.; Balzter, H.; Kaduk, J.; Tucker, C.J. Land degradation assessment using residual trend analysis of GIMMS NDVI3g, soil moisture and rainfall in Sub-Saharan west Africa from 1982 to 2012. *Remote Sens.* **2015**, *7*, 5471–5494. [CrossRef]
3. Kim, Y.; Kimball, J.S.; Zhang, K.; McDonald, K.C. Satellite detection of increasing Northern Hemisphere non-frozen seasons from 1979 to 2008: Implications for regional vegetation growth. *Remote Sens. Environ.* **2012**, *121*, 472–487. [CrossRef]
4. Truong, N.; Nguyen, H.; Kondoh, A. Land use and land cover changes and their effect on the flow regime in the upstream Dong Nai River basin, Vietnam. *Water* **2018**, *10*, 1206. [CrossRef]
5. Telesca, L.; Lasaponara, R. Discriminating dynamical patterns in burned and unburned vegetational covers by using SPOT-VGT NDVI data. *Geophys. Res. Lett.* **2005**, *32*, 1–4. [CrossRef]
6. Tucker, C.J.; Townshend, J.R.; Goff, T.E. African land-cover classification using satellite data. *Science* **1985**, *227*, 369–375. [CrossRef] [PubMed]
7. Richard, Y.; Poccard, I. A statistical study of NDVI sensitivity to seasonal and interannual rainfall variations in Southern Africa. *Int. J. Remote Sens.* **1998**, *19*, 2907–2920. [CrossRef]
8. Richard, Y.; Martiny, N.; Fauchereau, N.; Reason, C.; Rouault, M.; Vigaud, N.; Tracol, Y. Interannual memory effects for spring NDVI in semi-arid South Africa. *Geophys. Res. Lett.* **2008**, *35*, 195–209. [CrossRef]
9. Serrano, J.; Shahidian, S.; Marques da Silva, J. Monitoring seasonal pasture quality degradation in the Mediterranean Montado ecosystem: Proximal versus remote sensing. *Water* **2018**, *10*, 1422. [CrossRef]
10. Chang, J.; Tian, J.; Zhang, Z.; Chen, X.; Chen, Y.; Chen, S.; Duan, Z. Changes of grassland rain use efficiency and NDVI in Northwestern China from 1982 to 2013 and its response to climate change. *Water* **2018**, *10*, 1689. [CrossRef]
11. Martiny, N.; Richard, Y.; Camberlin, P. Interannual persistence effects in vegetation dynamics of semi-arid Africa. *Geophys. Res. Lett.* **2005**, *32*, L24403. [CrossRef]
12. Wu, D.; Zhao, X.; Liang, S.; Zhou, T.; Huang, K.; Tang, B.; Zhao, W. Time-lag effects of global vegetation responses to climate change. *Glob. Chang. Biol.* **2015**, *21*, 3520–3531. [CrossRef] [PubMed]
13. Iwasaki, H. NDVI prediction over Mongolian grassland using GSMaP precipitation data and JRA-25/JCDAS temperature data. *J. Arid Environ.* **2009**, *73*, 557–562. [CrossRef]
14. Huang, S.; Ming, B.; Huang, Q.; Leng, G.; Hou, B. A case study on a combination NDVI forecasting model based on the entropy weight method. *Water Resour. Manag.* **2017**, *31*, 3667–3681. [CrossRef]
15. Jahan, N.; Gan, T.Y. Modelling the vegetation-climate relationship in a boreal mixedwood forest of Alberta using normalized difference and enhanced vegetation indices. *Int. J. Remote Sens.* **2011**, *32*, 313–335. [CrossRef]
16. Schwinning, S.; Sala, O.E. Hierarchy of responses to resource pulses in arid and semi-arid ecosystems. *Oecologia* **2004**, *141*, 211–220. [CrossRef] [PubMed]
17. Eibedingil, I.; Casagrande, E.; Molini, A. An analysis of global climate-vegetation interactions over arid and semi-arid regions via causal statistics. *J. Cogn. Neurosci.* **2014**, *26*, 279–295.
18. Shoaib, M.; Shamseldin, A.Y.; Melville, B.W.; Khan, M.M. A comparison between wavelet based static and dynamic neural network approaches for runoff prediction. *J. Hydrol.* **2016**, *535*, 211–225. [CrossRef]
19. Bitzer, S.; Kiebel, S.J.; Bitzer, S.; Kiebel, S.J. Recognizing recurrent neural networks (rRNN): Bayesian inference for recurrent neural networks. *Biol. Cybern.* **2012**, *106*, 201–217. [CrossRef] [PubMed]

20. Chiang, Y.-M.; Chang, F.-J. Integrating hydrometeorological information for rainfall-runoff modelling by artificial neural networks. *Hydrol. Process.* **2010**, *23*, 1650–1659. [CrossRef]
21. Coulibaly, P.; Anctil, F.; Rasmussen, P.; Bobée, B. A recurrent neural networks approach using indices of low-frequency climatic variability to forecast regional annual runoff. *Hydrol. Process.* **2000**, *14*, 2755–2777. [CrossRef]
22. Smith, C.; Jin, Y. Evolutionary multi-objective generation of recurrent neural network ensembles for time series prediction. *Neurocomputing* **2014**, *143*, 302–311. [CrossRef]
23. Wu, Q.; Jin, Y.; Bao, Y.; Hai, Q.; Yan, R.; Chen, B.; Zhang, H.; Zhang, B.; Li, Z.; Li, X.; et al. Comparison of two inversion methods for leaf area index using HJ-1 satellite data in a temperate meadow steppe. *Int. J. Remote Sens.* **2015**, *36*, 5192–5207. [CrossRef]
24. Swaine, M.D. Rainfall and soil fertility as factors limiting forest species distributions in Ghana. *J. Ecol.* **1996**, *84*, 419–428. [CrossRef]
25. Ji, L.; Peters, A.J. A spatial regression procedure for evaluating the relationship between AVHRR-NDVI and climate in the northern great plains. *Int. J. Remote Sens.* **2004**, *25*, 297–311. [CrossRef]
26. Auerswald, K.; Wittmer, M.H.; Tungalag, R.; Bai, Y.; Schnyder, H. Sheep wool δ13C reveals no effect of grazing on the C3/C4 ratio of vegetation in the Inner Mongolia–Mongolia border region grasslands. *PLoS ONE* **2012**, *7*, e45552. [CrossRef] [PubMed]
27. Hasançebi, O.; Dumlupınar, T. Detailed load rating analyses of bridge populations using nonlinear finite element models and artificial neural networks. *Comput. Struct.* **2013**, *128*, 48–63. [CrossRef]
28. Waibel, A.; Hanazawa, T.; Hinton, G.; Shikano, K.; Lang, K.J. Phoneme recognition using time-delay neural networks. *Read. Speech Recognit.* **1990**, *1*, 393–404.
29. Rumelhart, D.E.; Hinton, G.E.; Williams, R.J. Learning representations by back-propagating errors. *Nature* **1986**, *323*, 533–536. [CrossRef]
30. Zhang, S.L.; Chang, T.C. A study of image classification of remote sensing based on back-propagation neural network with extended delta bar delta. *Math Probl. Eng.* **2015**, *4*, 1–10. [CrossRef]
31. Zhang, X.M.; Chen, Y.Q.; Babri, H.A. Augmented TDNN for frequency and scale invariant sequence classification. *Neurocomputing* **2003**, *50*, 1–16. [CrossRef]
32. Chang, F.J.; Chen, P.A.; Lu, Y.R.; Huang, E.; Chang, K.Y. Real-time multi-step-ahead water level forecasting by recurrent neural networks for urban flood control. *J. Hydrol.* **2014**, *517*, 836–846. [CrossRef]
33. Smith, J.A. LAI inversion using a back-propagation neural network trained with a multiple scattering model. *IEEE Trans. Geosci. Remote Sens.* **1993**, *31*, 1102–1106. [CrossRef]
34. Lin, T.; Horne, B.G.; Giles, C.L. How embedded memory in recurrent neural network architectures helps learning long-term temporal dependencies. *Neural Netw.* **1998**, *11*, 861–868. [CrossRef]
35. Chang, F.J.; Chen, P.A.; Liu, C.W.; Liao, V.H.C.; Liao, C.M. Regional estimation of groundwater arsenic concentrations through systematical dynamic-neural modeling. *J. Hydrol.* **2013**, *499*, 265–274. [CrossRef]
36. Wang, J.H.; Wang, S.P.; Schnug, E.; Haneklaus, S.; Patton, B.; Nyren, P. Competition between Stipa grandis and Cleistogenes squarrosa. *J. Arid Environ.* **2008**, *72*, 63–72. [CrossRef]
37. Rivas-Arancibia, S.P.; Montaña, C.; Hernández, J.V.; Zavala-Hurtado, J.A. Germination responses of annual plants to substrate type, rainfall, and temperature in a semi-arid inter-tropical region in Mexico. *J. Arid Environ.* **2006**, *67*, 416–427. [CrossRef]
38. Shivanna, K.R.; Tandon, R. *Reproductive Ecology of Flowering Plants: A Manual*; Springer: Berlin/Heidelberg, Germany, 2014.